Step-type and step-density influences on CO adsorption probed by Reflection Absorption Infrared Spectroscopy (RAIRS) using a curved Pt(1 1 1) surface

A.J. Walsh,[1,2,a] R. van Lent,[1,2] S.V. Auras,[1] M.A. Gleeson,[2] O.T. Berg,[3,b] and L.B.F. Juurlink[1]

[1] *Leiden Institute of Chemistry, Leiden University, PO Box 9502, 2300 RA Leiden, The Netherlands*

[2] *FOM Institute DIFFER (Dutch Institute For Fundamental Energy Research), P.O. Box 6336, 5600 HH Eindhoven, The Netherlands*

[3] *Department of Chemistry, California State University Fresno, Fresno, CA 93740 USA*

(Dated: 31 January 2017)

In comparison to flat single crystals, the continuous variation of structure provided by curved crystals offers many benefits for the study of physical and chemical processes at surfaces. However, the curvature of the surface also creates experimental challenges. For infrared spectroscopy in particular, adsorbates on metal samples are typically probed by grazing-incidence Reflection-Absorption Infrared Spectroscopy (RAIRS). In this geometry a convex crystal acts as a strongly diverging mirror. We describe how the experimental difficulties introduced by a cylindrical surface can be resolved for RAIRS. A complementary mirror, placed directly downfield of the curved crystal within the vacuum chamber, minimizes the divergence created by the sample. By simply translating the infrared focus across the sample, we probe adsorbate vibrational spectra as a function of local step-type and step-density with high sensitivity and spatial resolution. Time-consuming sample exchange, and the concomitant sample-to-sample experimental errors, are eliminated. We apply this new technique to carbon monoxide adsorption on a curved Pt(1 1 1) crystal and use it to resolve the influence of step-type and step-density on the CO stretch vibration as a function of coverage.

PACS numbers: Valid PACS appear here

Keywords: curved single crystal surface, cylindrical single crystals, Reflection Absorption Infrared Spectroscopy, RAIRS, IRAS, platinum, carbon monoxide

I. INTRODUCTION

Commercial heterogeneous metal catalysts contain a wide array of surface defects, such as adatoms, steps, and kinks. For several of the largest industrial processes, monatomic steps on catalyst particles have been shown to be crucial to the kinetics of the overall process.[1,2] Therefore, fundamental studies that use macroscopic single crystals to mimic actual catalyst particles need to include such defects. A single crystal can be cut to expose vicinal planes of well-characterized structure for this purpose. While low Miller index surfaces are most commonly studied, high Miller index surfaces—which expose regularly spaced straight or kinked steps separated by atomically flat terraces—can also be formed. Studies attempting to bridge the 'structure gap' between the ordered samples used in surface science and real catalysts were recently reviewed by Vattuone, Savio, and Rocca.[3]

Single crystals as model samples are generally studied under ultrahigh vacuum (UHV) conditions. UHV allows for a very large range of surface sensitive techniques.[4] However, the use of separately polished flat surfaces to probe the influence of different step types and/or terrace widths imposes difficulties[3]: sample-to-sample variation in the quality and purity of the surface and bulk of individual single crystals; the required breaking of vacuum; initial cleaning of new crystals, which may take months of sputtering-annealing cycles; and differences in absolute temperature measurement resulting from minor variations in thermocouple connections. Some problems can be overcome: repetitive breaking of UHV conditions can be eliminated through the use of a load-lock system, and the effect of different impurities between crystals can be removed (at least in part) by cutting all samples from the same single crystal boule. However, the expense and time necessary to work with multiple individual crystals remains. In our experience, the experimental time requirement is proportional to the number of surfaces studied.

An alternative approach is to exploit the variety of step types, step densities, and terrace types offered by a single crystal that is not flat. Various shapes have been utilized, including fully cylindrical crystals, which exhibit at least two regions of each low Miller index structure on its circumference;[5–7] and dome-shaped crystals, which also include kinked step edges.[8,9] For a nickel cylin-

[a] Electronic mail: a.j.walsh@lic.leidenuniv.nl
[b] Electronic mail: oberg@csufresno.edu

der with its rotational axis along (1 1 0), we found mostly smooth variations in step density between the three low Miller index surfaces (1 0 0), (1 1 1), (1 1 0).[10] In contrast, faceting of high Miller index planes was observed on a cylindrical Pt crystal oriented with its rotational axis along (1 0 0).[7] Limitations of working with a full cylindrical crystal include the thermal inertia of a large sample, and the difficulty of adapting sample holders to this shape. A compromise solution is to fashion a section of curved crystal into the approximate size and shape of a typical flat sample. Although the range of surface structures available on such a partial section is limited, such crystals have been employed successfully in standard UHV systems.[11,12] Generally, the direction of curvature is chosen such that the curvature results from atomically straight step edges. Dome-shaped crystals offer a continuous range of surface structures, including straight and kinked step edges.

Studies employing curved crystals must use diagnostic techniques with sufficient spatial resolution; this factor is unimportant to the majority of studies on flat crystals. Focused electron or ion beams, for example, have been applied to probe the continuously changing surface structure with high spatial resolution. Early studies employed various techniques, e.g., Low Energy Electron Diffraction (LEED),[10,13] Auger Electron Spectroscopy (AES)[14,15] and Photoelectron emmission microscopy (PEEM).[7] More recently Scanning Tunneling Microscopy (STM)[11,16,17] and probes using electromagnetic radiation, e.g., Angle Resolved Photoemission Spectroscopy (ARPES),[16,18] and X-ray Photoelectron Spectroscopy (XPS),[11] have been shown to be applicable with high spatial resolution. These techniques mostly probe the chemical identity, oxidation state, and electronic states of the surface and its adsorbates. The dynamics of chemical processes were studied using supersonic molecular beams. In this way, the King & Wells technique was used to determine the absolute probability of molecular and dissociative adsorption as a function of incidence angle and kinetic energy.[5] Also, spatially-resolved temperature programmed desorption (SR-TPD) has demonstrated differences in the desorption of H_2O from different step types of a curved Ag(1 1 1) single crystal.[12]

A vibrational probe is ideal for the identification of molecular adsorbates and reaction intermediates. In RAIRS, the adsorbate's vibrational spectrum is used for *in situ* identification, and as a probe of the local environment.[19] Typically a flat crystal under vacuum is placed between the interferometer and detector of a commercial Fourier Transform Infrared (FTIR) spectrometer. The absorption bandshape and oscillator strength carry information on the structure and chemical environment of adsorbates—most importantly, relative coverage and the nature of adsorption sites, (e.g., linear (on-top), double-bridge or multi-bridge (hollow), and high- or low-coordination sites can be identified.[19,20] Further benefits include ease of instrumentation, rapid acquisition time (commonly less than 30 s), and high energy resolution (typically 2 cm^{-1}, $< 0.1\%$ of a stretching vibration). RAIRS is a prominent technique in surface science;[21,22] however, it can not be used for curved surfaces without modification.

In the present work, a routine RAIRS set-up is adapted to incorporate a curved single crystal. The experimental details are described in II and the concept and design in III. A summary of previous reported CO/Pt behavior is given in IV, followed by sample spectra of CO adsorbed to a Pt curved crystal, along with LEED analysis, in V. Measured spectra are discussed in VI. Finally, a brief conclusion of the overall work is given.

II. EXPERIMENTAL DETAILS

Experiments were performed in an UHV chamber with a base pressure of $2 \cdot 10^{-10}$ mbar. The UHV chamber is equipped with a LEED/Auger system (VG, RVL-900), a quadrupole mass spectrometer (Pfeiffer, QMA 200), and an external Fourier transform infrared spectrometer (Bruker, Vertex 70) for RAIRS.

The curved platinum crystal (Surface Preparation Lab, Zaandam, the Netherlands) is similar to a curved Ag(1 1 1) crystal described previously.[12] The sample can be pictured as a thin circular section normal to the axis of a complete cylinder; this parent cylinder has its axis in the (1 1 0) direction and a radius of $r = 15.0$ mm. The section is 8 mm in diameter, therefore it encloses 31° of cylindrical azimuth, chosen such that the apex is a (1 1 1) plane of the FCC structure of bulk Pt. The curvature is created by spark erosion and sanding, after which the surface is polished in an automated, custom-built polishing machine (Surface Preparation Lab, Zaandam, the Netherlands). The curvature of the crystal imposes a gradual increase in monatomic step density[11] as a function of azimuthal distance from the apex. The (1 1 1) terraces are separated by (1 0 0) (A-type) steps on one half of the crystal, and (1 1 0) (B-type) steps on the other half. Thus the crystal encompasses surface structures ranging from Pt(5 3 3) at $-14.4°$ to Pt(5 5 3) at $+12.3°$.

The crystal is mounted in a square tantalum holder, which is encapsulated in Pt foil to prevent contributions from tantalum. The crystal holder is suspended from a liquid nitrogen cooled cryostat on a x, y, z, ϕ manipulator. The liquid nitrogen level is kept at roughly 50% to avoid contraction or expansion of the cold finger and consequential motion of the crystal. The sample holder is electrically isolated from the cryostat and the rest of the machine by AlN plates. The crystal is heated by radiative heating and electron bombardment using a filament (Osram, 150 W). High temperatures (> 600 K) are

achieved by applying a positive bias to the crystal. The crystal is cleaned through multiple cycles of Ar^+ sputtering (Messer, 5.0; 400 K; 0.5 μA; 45°; 10 min; 0.25 kV), followed by O_2 treatment (Messer, 5.0; $3.5 \cdot 10^{-8}$ mbar; 900 K; 3 min) and *in vacuo* annealing (1200 K; 3 min). Three cleaning cycles were performed every day prior to measurements. The surface structure was checked using LEED. The sample was annealed for 3 min at 1200 K between individual measurements to ensure the quality of the surface.

III. CONCEPT AND DESIGN

Schematics of the system are displayed in Figure 1(a), (b) and (c). Because s-polarized light does not contribute to absorption at a metal surface, RAIRS measurements are performed at grazing incidence (roughly 85°) using p-polarized light. We follow the usual implementation by placing the sample at the focus of a paraboloid represented by two 90° off-axis mirror segments ($f = 203$ mm) outside of the vacuum chamber: one to focus the FTIR beam onto the sample, and one to re-collimate it for eventual imaging at the detector. The crystal is oriented with its cylindrical axis horizontal, in the optical plane of incidence. Therefore it does not affect imaging in the plane of incidence, an effective focal length (f) of infinity, but scatters optical power out of the plane of incidence ($f = -7.5$ mm). This expansion is eliminated by a concave cylindrical mirror downfield of the sample; the mirror is coaxial with the sample, but has a focal length that is greater ($f = 8.0$ mm) by the transverse distance separating the sample and mirror, 1.0 mm. The pair therefore act as an anamorphic beam expander. The effect is to translate the optic axis by 1.0 mm in the plane of incidence, and to magnify the beam by 16/15 normal to the plane of incidence. An advantage of this double-reflection geometry over the traditional RAIRS setup is that the sample introduces no angular deviation to the infrared beam; therefore the spectrometer and detector can be aligned without the sample present. The focus quality on the sample is determined entirely by alignment of the upstream paraboloid. Misalignment of the collimator can at worst distort the source image enough that it spills over the detector element, and thereby reduces the infrared throughput and sensitivity. In practice the double-reflection throughput was comparable to the no-sample throughput. The mirror is a fused-silica substrate evaporatively coated with gold; an image of the mirror and crystal is shown in Figure 1(d).

Inside the UHV chamber, both the coaxial collimator and the sample holder are connected to the cryostat and consequently move in tandem. The collimator is connected to the cold finger, which is isolated from the crystal holder, thereby protecting it from elevated temperatures. The centers of the sample and 12 mm × 15 mm

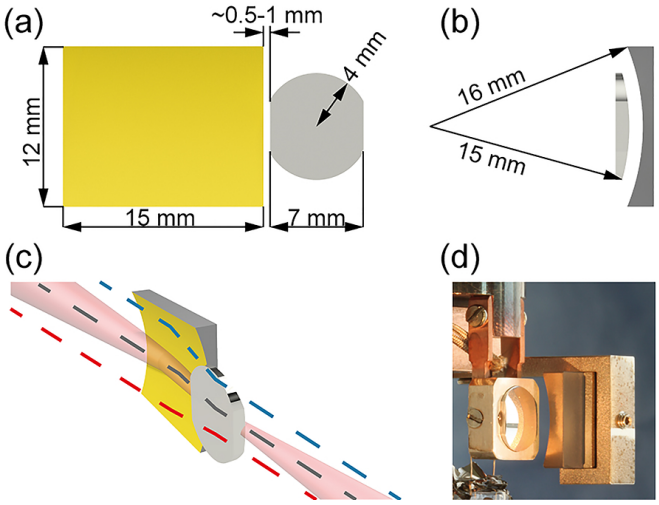

FIG. 1. (a) A frontal view, facing the gold co-axial collimator and back of the curved platinum crystal. The gold collimator is placed approximately 0.5 to 1 mm after the crystal on the detector side, hence they do not overlap. (b) An axial view of co-axial collimator and curved crystal surface. The surfaces are separated by 1.0 mm in the radial direction (c) A guide to the eye of the path, beginning on the right, of IR light as it passes through an aligned set-up. Any extra divergence as a result of the curved platinum surface is corrected for by the co-axial collimator. The dashed lines represent example HeNe laser beam paths used for alignment (d) A perspective image of the adapted crystal holder, facing the platinum curved surface.

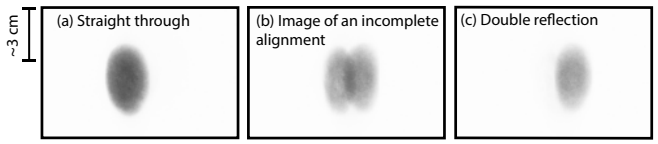

FIG. 2. Gray scale images formed on white paper placed 2.5 m from a parabolic mirror at the exit window of the chamber when (a) light travels through the gap between surfaces, (b) when light begins to reflect off both surfaces and (c) a clear double reflection. The light source is a circular pinhole placed in front of a standard tungsten filament of the spectrometer.

mirror are offset by approximately 12 mm along the optic axis, hence they do not overlap in the surface-normal direction. Alignment of the collimator relative to the crystal surface is performed outside vacuum using a HeNe laser.

Because the sample is oriented with its cylindrical axis in the optical plane of incidence, the infrared footprint is elongated in the axial direction, along which there is no variation in surface structure. Regions of different step density are reached by raising or lowering the entire cryostat/sample/collimator assembly. The alignment process is aided by a selectable tungsten filament light source inside the spectrometer. This source creates a visible-light replica of the IR beam that is used for alignment and the

beam path does not change once set. After locating the correct axial position of the infrared focus, alignment in the transverse direction is also necessary to compensate for the curvature of the surface and to obtain a pure double reflection at each vertical position. This is achieved by translating the sample across the visible beam until only the double reflection can be observed. Figure 2 shows three images observed 2.5 m after the exit window of the chamber when light travels through (a) the gap between surfaces, observed as a single vertical ellipse, (b) when a portion of the light reflects off the platinum and gold surfaces, resulting in the appearance of a second vertical ellipse alongside, and (c) a clear sample double reflection, where only the reflected vertical ellipse can be seen.

To determine the correct vertical positions, the crystal is placed parallel to the beam path and translated horizontally and vertically, while at the same time observing the intensity of transmitted light. When the intensity reaches a sharp minimum in the vertical, the beam focus is incident on the apex of the crystal, as the sample extends further into the beam path the minimum broadens. Once the apex has been determined, positions of different vicinal regions are located using previously determined values of Van Hove and Somorjai.[23] In the present setup, the position of the manipulator can be adjusted in steps of 10 μm in the vertical plane and in steps of 5 μm in the horizontal plane. Background spectra were recorded at each crystal position.

While unimportant for many flat single crystals, the spatial resolution of diagnostic tools is essential when working with curved surfaces since it defines the range of structures probed. To determine the spatial resolution, we assume a Gaussian beam profile and measure the beam width at the sample position using the "*knife edge*" technique. The crystal is replaced by a knife edge placed perpendicular to the incident beam path. By moving the knife edge into the beam path in steps and measuring the transmission at each step, the spatial resolution can be measured at different positions along the beam path.[24] At the crystal center, the beam was determined to have a FWHM = 0.72 mm. This value represents the source pinhole as magnified by the collimator within the FTIR and the sample focus paraboloid. If necessary, higher spatial resolution can be achieved. The simplest technique is to focus IR light of the globar on a smaller pinhole. Higher resolution can also be achieved by focusing light of the globar onto an optical fiber, instead of a pinhole. The optical fiber removes the image of the globar and consequently the focus of the light exiting the optic fibre is tighter than it would be for a pinhole of the same size. A number of optic fiber IR sources are available commercially[25].

IV. SUMMARY OF PREVIOUS STUDIES WITH CO ON BOTH FLAT AND CURVED PLATINUM SINGLE CRYSTALS

CO on platinum is a thoroughly studied model system—a prototype of fundamental processes at catalytic metal surfaces.[26,27] Low CO coverages on Pt(1 1 1) form a $(\sqrt{3}\times\sqrt{3})$R30° structure, with CO chemisorbed carbon down atop platinum atoms. Increasing CO coverage results in the occupation of bridge sites,[28–30] while the structure evolves to a mixed atop/bridge c(4×2).[28,31] Scanning tunneling microscopy (STM) images have observed the evolution of low on-top CO coverage to $(\sqrt{3}\times\sqrt{3})$R30° hexagonal island superstructure, and the later formation of rectangular c(4×2) domains.[32] In the range 0.3 to 0.5 ML, RAIRS has played a crucial rule in the identification and study of the evolution of overlayer structure, thanks to the strong sensitivity of the atop-adsorbed line shape to structural homogeneity of the adsorbate layer.[33,34]

On higher Miller index vicinal surfaces, on-top and bridge sites at step edges are populated. However, in contrast to Pt(1 1 1) infinite terraces, terraces on stepped surfaces often do not contain equal bridge and on-top site occupation at saturation. This functionality is a consequence of the limitations imposed by finite terraces on possible superstructures.[35] On-top step sites are the most favorable initial location,[35–39] followed by bridge step sites.[38] Once bridge and on-top step sites are fully occupied, increasing CO coverage follows the same pattern as Pt(1 1 1). CO adsorbed on a Pt(1 1 1) terrace has a low barrier to lateral diffusion. Consequently, migration of CO from the terrace to the thermodynamically favorable strong binding step can occur below 100 K, the minimum surface temperature of the present work.

The effects of A- and B- type steps on bridge and on-top binding energies have been studied with XPS.[38] Tränkenschuh *et al.* compared Pt(3 2 2) and Pt(3 5 5), both of which contain 5 atom wide (1 1 1) terraces but differing step types, A- and B- respectively.[38] On A-type steps, both bridge and on-top adsorption sites were occupied, whereas on B-type steps only on-top sites were observed. Accordingly, higher step coverage was observed on B-type steps. By TPD analysis of the platinum samples, it was found that the on-top CO was bound more strongly to the B-type steps. On A-type steps, the binding to the bridge was found to be weaker than to the on-top. Relative occupation for step and terrace sites as a function of coverage and temperature were also found to differ with step type. On Pt(3 5 5), little effect was observed. Whereas on Pt(3 2 2), large changes were observed with temperature at a given coverage. This can be attributed to contrasting interactions due to binding energy differences on step types.

One previous study of CO on a curved Pt crystal

has been reported by Walter *et al.*.[11] The single crystal used was a cylindrical section cut and polished around a Pt(1 1 1) plane, containing families of step densities for both A- and B-type steps, the same crystal design as presented here. Using XPS with a spatial resolution of 100 μm, the preferred CO site occupation (i.e. terrace vs. step and bridge vs. on-top) was observed, confirming the previously reported hierarchy. No change of absolute coverage was found for terrace length or step type as a function of dose. However, the distribution of adsorption sites did change. The diffusion of CO from terraces to steps was measured as a function of terrace length for different dosages. The curved surface and XPS diagnostic was also used to accurately determine room temperature CO saturation at different dosages.

RAIRS is an especially effective diagnostic for the study of CO on platinum surfaces, due to the molecule's strong stretching mode and sensitivity to the manner in which it is bonded to the surface, resulting in strong absorptions and distinguishable frequency shifts in combination with the benefit of all *ex-situ* optical spectroscopy.[19,20,33–35] The experimental parameters (0.72 mm beam waist and 7 cm^{-1} instrument function) are a compromise between light intensity, spatial resolution, and spectral resolution.

V. SAMPLE MEASUREMENTS OF CO ON A CURVED PLATINUM CRYSTAL

A. LEED analysis

LEED analysis was used to determine surface structure and consequently different vicinal regions, nine in total, on the curved surface. LEED diffraction patterns of stepped arrays determined terrace width and step height. By translating the crystal normally to the incident electron beam, an evolution of spot splitting occurs in the LEED pattern.[10] The evolution divided by row spacing in the LEED pattern as a function of angle from apex is plotted in Figure 3(b), along with theoretical values. The step type, terrace width and Miller index of vicinal regions studied using RAIRS are shown in Table I. The spot splitting/row spacing ratios observed at these surfaces agree with those previously determined by Van Hove and Somorjai.[23] A plot of these ratios as a function of angle measured from the platinum crystal is also shown in Figure 3(b).

B. Absorbance spectra of CO

Light attenuation is described with the Beer-Lambert Law, $I = I_0 e^{-\sigma a}$. I_0 and I are transmission intensities through the optical set-up. I_0 measured after reflection off a clean surface and I measured following reflection off a CO covered surface. σ and a are the absorption cross-section of CO (in units of m^2) and surface density of CO (in units of m^{-2}). In the case of low- or high-Miller index flat single crystals, CO can sit in multiple positions, see IV, forming an anisotropic distribution on the surface, while the platinum surface forms an isotropic surface in both low- and high- miller index surfaces. In a simple application of the Beer-Lambert law, the individual contribution of different states is ignored and σ is an effective frequency dependent absorption cross-section, linearly proportional to the sum of individual contributions. The CO molecules do not interact and are dispersed over a featureless flat surface. In the case of a curved crystal, the crystal surface itself is inhomogeneous perpendicular to the cylindrical axis and due to the finite size of the IR beam, absorption from a range of step types and terrace lengths occurs. We apply the Beer-Lambert law in the same manner, a is the surface density of CO on a flat featureless surface and σ is an effective absorption of a non-interacting molecule. However, implicit insight from many systematic changes in spectra as a function of step type and density, such as oscillator strengths and frequency shifts, can be found, see below VI.

Tighter IR beam spatial resolution and a high number of vicinities extracts detail most efficiently. However, the observation of absorption signal, due to low surface coverage and/or weak oscillator strengths, may require a reduction in the beam resolution and consequently an overlap between the tails of beam footprints in adjacent step-density vicinities being studied. Despite this overlap, differences in spectra are still observed, as each IR beam covers a different range of continuously evolving step-densities, and important systematic changes can still be detected. See for example the distinct differences in the CO on-top vibrational peaks measured at the adjacent (9 7 7) and (11 9 9) positions as shown in Figure 3.

Background transmission spectra of the clean surface were obtained at each crystal position. Subsequently, a 0.75 L (100 s at 1×10^{-8} mbar) CO dosage at 100 K platinum surface temperature was implemented. Absorption centred at 9 positions on the crystal, see Table I, was measured. Four samples of each step type was measured individually, with terrace lengths of 4, 5, 8 and 10 atoms, as well as the center of the crystal containing the (1 1 1) plane. Sample spectra are presented in three figures. Figure 3(d) shows two absorbance spectra of on-top CO for each position. Each spectrum was measured at 100 K, after flashing the crystal to 300 K (red) and 400 K (black). Figure 4 presents a measurement of more temperature dependence and compares on-top spectra after desorption of CO at different temperatures for (11 9 9) and (5 5 3) surfaces. Figure 5 presents absorbance spectra including bridge and on-top features.

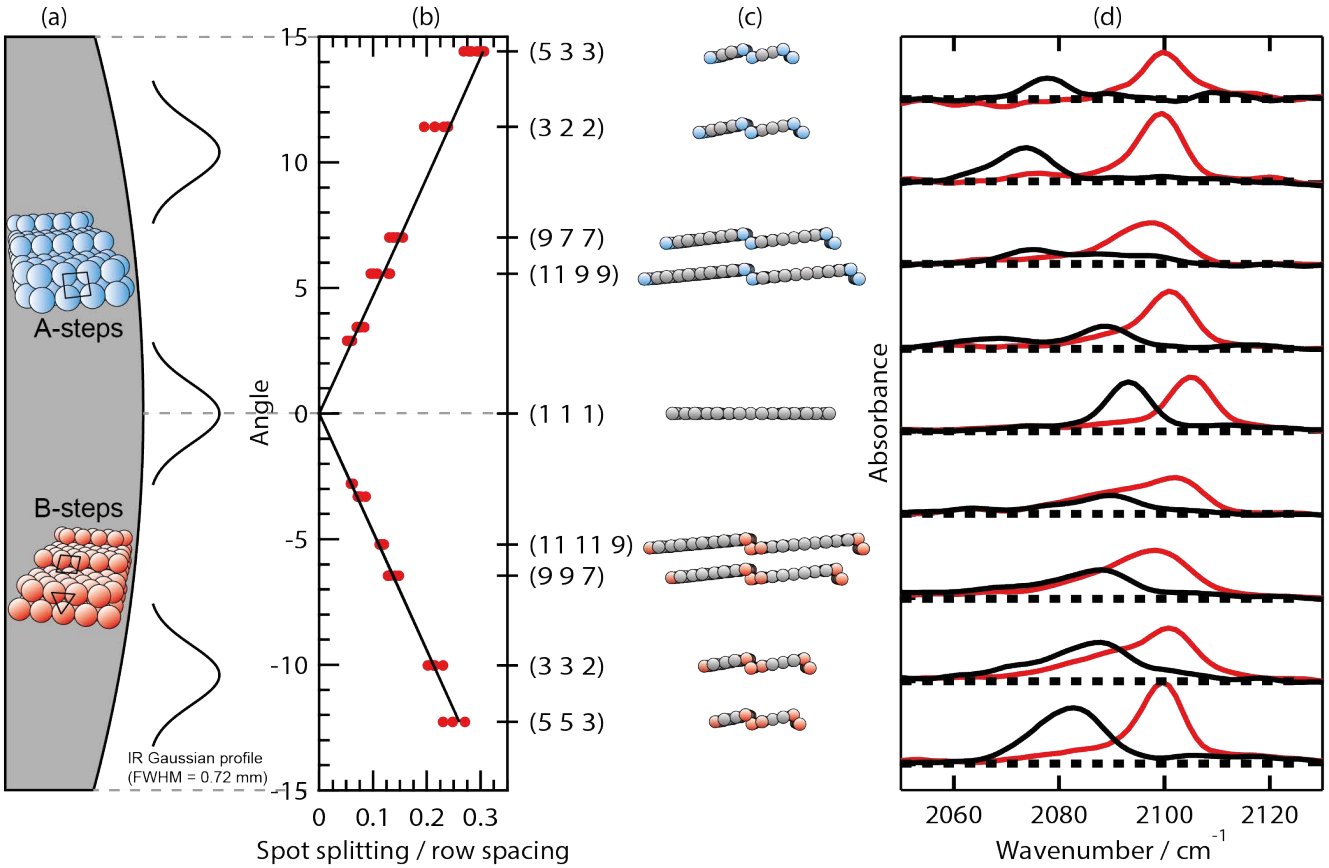

FIG. 3. (a) Curved platinum single crystal surface. Crystal center contains a (1 1 1) infinite plane. On either side are A and B type steps, with (1 1 1) terrace lengths (thus step density) increasing with displacement from the center. (b) The ratio of LEED spot splitting to row spacing can be used to locate positions on the crystal where a specific step type and terrace length are located. The positions of the surface structures are dependent on the angle from the (1 1 1) infinite plane. (c) Locations of terrace lengths extracted from LEED data. (d) RAIRS spectra of the on-top CO vibrational band measured at surface structures shown in (c). Before measurement, the surface was saturated with CO while at a surface temperature of 100 K. Subsequently, RAIRS spectra were recorded at each position, after flashing the surface to 300 K (red) and 400 k (black). From the RAIRS spectra recorded, a clear difference between CO behavior on different surface structures can be observed.

Terrace length (atoms)	4	5	8	10	Infinite
Step type A	(5 3 3)	(3 2 2)	(9 7 7)	(11 9 9)	(1 1 1)
Step type B	(5 5 3)	(3 3 2)	(9 9 7)	(11 11 9)	(1 1 1)

TABLE I. Miller index of vicinal regions studied. Terrace lengths and step types are also indicated.

Any possible contribution from CO adsorption on the gold co-axial collimator is monitored by regularly measuring transmission spectra off clean platinum crystal surfaces. For each vicinal region, transmission was measured before each CO dosage. Due to attachment of the co-axial collimator directly to the cold finger, any adsorption of CO on the gold surface during the CO dosage will remain constant throughout the measurement for that vicinal region. Having finished a measurement, CO has desorbed from the platinum surface. A transmission spectrum is measured off the clean platinum crystal. This spectrum is used as the background for spectra. From difference transmission spectra of before and after measurement of a specific vicinal region, no features suggesting CO coverage on the gold surface were observed within the sensitivity of our measurements.

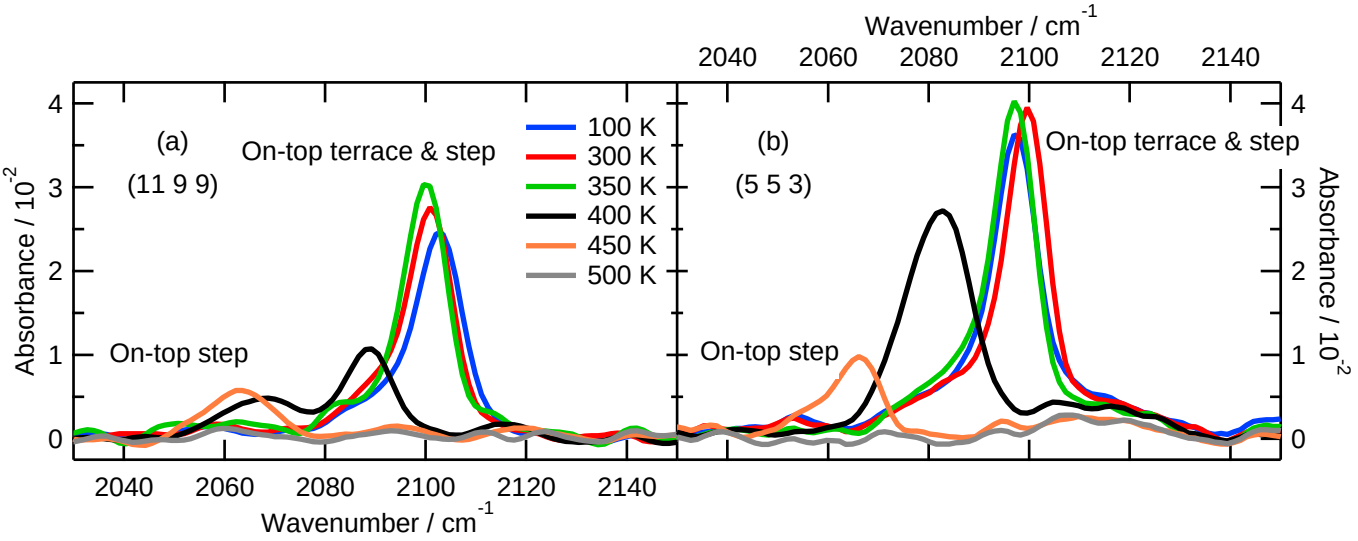

FIG. 4. Absorbance spectra of the on-top CO vibrational band on; Panel (a) (11 9 9) and Panel (b) (5 5 3). For each surface a 0.75 L CO dosage was used at 100 K surface temperature. Spectra were measured after flashing sequentially to 300 K, 350 K, 400 K, 450 K and 500 K. All spectra were recorded at 100 K. Initially a single band peak is observed from step and terrace site occupation. Sequential flashing the crystal to higher temperatures results in the reduction of CO on the terrace. Consequentially, the band begins to shift towards lower wavenumbers and in the case of (11 9 9), a second band appears. When only step sites are occupied, a single band is observed, with a peak at the lowest wavenumber measured.

VI. ANALYSIS AND DISCUSSION OF THE CO ON PLATINUM SPECTRA

A. Absorbance spectra of CO on-top sites

Terrace and step on-top sites yield different internal vibrational frequencies, separated by 20 cm^{-1}.[35,40] At the step, positive outward dipoles split the molecular orbitals of the adsorbed CO, resulting in a lowering of the $2\pi^*$ orbital energy.[36,41] This increases back donation from Pt to CO, and consequently CO bonded to the step edge has a lower frequency than on the terrace.

Band peak positions on all surfaces after flashing to 300 K are located between 2097 cm^{-1} and 2104 cm^{-1}; 2100 cm^{-1} is the accepted peak position for a saturated Pt(1 1 1) surface.[42–44] Previous studies have reported both on-top terrace and step sites to be occupied at high coverages.[35,36,38,44] Only single bands are observed at high coverage, however, because transition-dipole/transition-dipole coupling yields delocalized molecular excitons. The majority terrace-site resonance falls within the natural linewidth of the minority step resonance, hence the latter donate their oscillator strength to the single excitonic signal. Step density determines the number of each sub-population contributing to the exciton, and thereby modulates the band frequency and intensity. At the extremes of either no steps or high step density, the adsorbed layer is relatively uniform within the typical delocalization distance, and yields a narrow resonance. At intermediate step densities the step-adsorbed molecules are effectively defects in the terrace-adsorbed exciton, and the resonance is broadened. The integrated absorbance (hence infrared oscillator strength) is approximately conserved, but the tilt and modified electronic structure of edge-adsorbed molecules could account for systematic changes.

Flashing the crystal to 400 K creates a much higher diversity in signal— 2073 cm^{-1} to 2093 cm^{-1}—as a function of step density. All vibrational bands shift toward lower frequencies, and in some cases two peaks are resolved. When flashing, CO is desorbed from the layer in the order of increasing adsorption energy: terrace bridge sites first, terrace on-top sites after, then A- and B-step sites.[35,36,38] As expected, the integrated absorbance at Pt(1 1 1) is reduced slightly by this loss of molecules. The band center is also shifted, an indication that the terrace-adsorbed layer is not present as constant-density islands, since the magnitude of transition-dipole/transition-dipole coupling within such islands would be independent of coverage. Once again areas of intermediate step density yield broad spectra characteristic of excitons in a non-uniform layer. At high step density and low coverage, the absorption band narrows again. This resonance must represent a molecule uniformly bound to step sites and decoupled from the terrace-site exciton, which is now depopulated. Sensitivity permitting, an unambiguous assessment of intermolecular coupling effects would require isotopomeric dilution measurements. Examples of detailed RAIRS analysis can be found in Hollins[44] and Hoffmann.[19]

In agreement with the literature, there is a preferential retention of molecules at the strongly-binding B-type

steps.

Figure 4(a) and (b) displays the absorbance of on-top CO on surfaces (11 9 9) and (5 5 3), following a 0.75 L dosage at 100 K. Spectra were measured at 100 K, and then sequentially after flashing to 300 K, 350 K, 400 K, 450 K and 500 K. All spectra were recorded at 100 K. Measurements on (11 9 9), where the terrace width is 10 atoms separated by A-type steps, show clearly the gradual separation of step and terrace absorbance bands as the latter sites are depopulated. Flashing the (11 9 9) crystal surface to 300 K and 350 K has little effect on the peak band position, shifting it in steps of 4 cm^{-1}. This small shift is due to the desorption of CO from the terrace, resulting in larger intermolecular distances of CO on the terrace. The integrated absorbance increases, possibly due to ordering of the terrace-bound layer.[36] After flashing to 400 K, and the presumed loss of most terrace-bound molecules, two distinct red-shifted peaks appear. Only a single band at 2063 cm^{-1} remains after flashing to 450 K, indicating that only step sites are populated. After a cycle to 500 K the coverage falls below the detection sensitivity of our experiment.

Due to the higher step density, resulting in a stronger on-top step dipole compared to the terrace, the peak position at 100 K of (5 5 3) is closer to the on-top step singlet frequency than (11 9 9). The behavior of (5 5 3) on-top spectra follows the same pattern as (11 9 9), except after flashing to 400 K. The band position shifts to the red, but no distinct on-top step band is observed and the band width increases only slightly. This behavior may reflect the greater similarity of B-type steps to a (1 1 1) terrace.

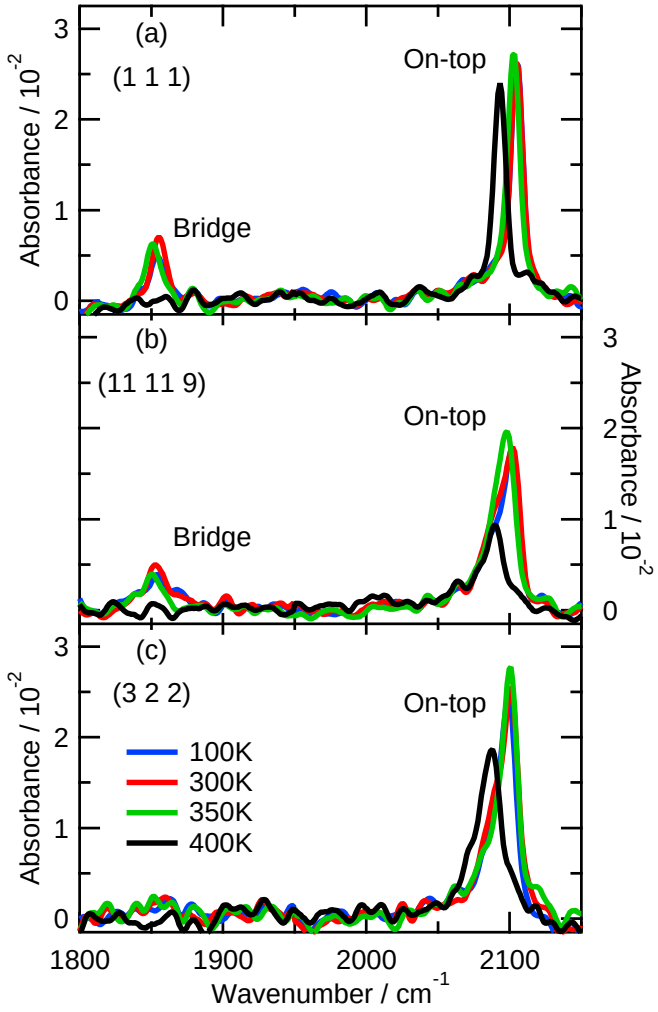

FIG. 5. Absorbance spectra of CO including on-top and bridge signals. Panels (a), (b) and (c) contain spectra for (1 1 1), (11 11 9) and (3 2 2) vicinal regions respectively. For each surface a 0.75 L CO dose was used at 100 K surface temperature. Spectra were measured directly after dosing and sequentially after flashing to 350 K and 400 K. All spectra were recorded at 100 K.

B. CO sitting on a twofold bridge

CO in a bridge position has a smaller infrared cross-section than CO in an on-top position.[35,36] Figure 5 compares absorbance spectra measured on (1 1 1), (11 11 9) and (3 2 2) surfaces at 100 K. Figure 5(a) shows the absorbance of a (1 1 1) surface, on which 50% of CO molecules are in bridge sites;[28,45] the integrated absorbance of the bridge-bound population is more than four times smaller than the on-top signal. After annealing the (1 1 1) surface to 350 K, the bridge signal remains. Subsequent annealing to 400 K removes the bridge signal, as previously reported. Figure 5(b) shows CO on the (11 11 9) surface, with 10-atom wide (1 1 1) terraces separating B-type monatomic steps. Here the bridge signal appears broader than on (1 1 1), due to vibration-vibration coupling between CO positioned on steps and terraces. The terraces are depleted by annealing to 350 K, and the bridge signal narrows accordingly. After annealing to 400 K, the bridge-bound signal falls below the experimental sensitivity.

Figure 5(c) shows the (3 2 2) surface, with five-atom wide terraces separated by monatomic A-type steps. On the (3 2 2) surface, CO bridge signal is not detected under any conditions, even though it has previously been reported by Tränkenschuh *et al.*.[38] In all cases of four- or five-atom wide terraces, no CO signal is visible. In some cases, it may be due to reorientation of CO on shorter terraces, and the resulting lower density of occupied bridge sites. A second reason may be weaker absorption coefficients on the shorter terraces. Any tilting of molecules away from the surface normal would reduce the transition dipole strength perpendicular to the surface and lower the integrated absorbance, and increasing the density of steps would increase the density of such tilted bridging molecules. Bridge signals on narrower terraces have been

reported. We speculate that CO adsorbed to bridge sites in higher step-density vicinal regions are at a quantity too low to be observed in the current set-up. However, a number of steps can be taken to improve signal. To increase the area being investigated without increasing the range of vicinal regions being explored, a slit aperture could be used as a light source instead of a pinhole. The greater area of the slit would increase IR throughput without a loss of spatial resolution. Sensitivity can also be improved by a more intense IR source, such as a cooled globar.

VII. CONCLUSION

Curved single crystals provide a continuous range of high- and low- index vicinal regions on a single surface. Yet the use of these crystals in surface science experimental systems can prove difficult, as the majority of diagnostic tools have been developed for flat surfaces and low spatial resolution. The use of RAIRS in particular is hindered by the curved surface acting as a powerful diverging mirror inside the chamber. By placing a co-axial collimating mirror after the sample, we have modified a standard UHV RAIRS set-up to allow the use of curved surfaces. The collimator is aligned to minimize the expansion of the infrared beam created by the curved crystal surface. We have presented proof-of-principle measurements on a curved platinum crystal containing a family of A- and B- type steps separated by (1 1 1) terraces. Spectra were measured for a variety of CO coverages on nine different positions on the crystal. Four terrace widths (4, 5, 8 and 10 atoms wide), with separate A- and B-type steps, were investigated, as well as the (1 1 1) surface. Both on-top and bridge CO sites were observed, and their behavior as a function of temperature was consistent with published work on this classic system. A study of nine surface types using individual flat single crystals could take nine times as long as the experiments presented here.

ACKNOWLEDGMENTS

The authors gratefully acknowledge the support from Netherlands Organisation for Scientific Research (NWO), grants. Technical support from Thijs Hoogenboomand, Peter van Veldhuizen and Raymond Koehler is greatly appreciated.

[1] K. Honkala, A. Hellman, I. Remediakis, A. Logadottir, A. Carlsson, S. Dahl, C. H. Christensen, and J. K. Nørskov, Science **307**, 555 (2005).
[2] M. Behrens, F. Studt, I. Kasatkin, S. Kühl, M. Hävecker, F. Abild-Pedersen, S. Zander, F. Girgsdies, P. Kurr, B.-L. Kniep, *et al.*, Science **336**, 893 (2012).
[3] L. Vattuone, L. Savio, and M. Rocca, Surface Science Reports **63**, 101 (2008).
[4] G. Somorjai, Catal. Lett. **7**, 169 (1990).
[5] C. Hahn, J. Shan, Y. Liu, O. Berg, A. W. Kleijn, and L. B. Juurlink, J. Chem. Phys. **136**, 114201 (2012).
[6] G. Veser, P. A. Thiel, and R. Imbihl, J. Phys. Chem. **98**, 2148 (1994).
[7] M. Sander, R. Imbihl, R. Schuster, J. Barth, and G. Ertl, Surf. Sci. **271**, 159 (1992).
[8] T. Lawton, V. Pushkarev, D. Wei, F. Lucci, D. Sholl, A. Gellman, and E. Sykes, J. Phys. Chem. C **117**, 22290 (2013).
[9] A. J. Gellman, W. T. Tysoe, and F. Zaera, Catal. Lett. **145**, 220 (2015).
[10] R. V. Mom, C. Hahn, L. Jacobse, and L. B. Juurlink, Surf. Sci. Rep. **613**, 15 (2013).
[11] A. L. Walter, F. Schiller, M. Corso, L. R. Merte, F. Bertram, J. Lobo-Checa, M. Shipilin, J. Gustafson, E. Lundgren, P. Cabrera-Sanfelix, *et al.*, Nat. Commun. **6**, 8903 (2015).
[12] J. Janlamool, D. Bashlakov, O. Berg, P. Praserthdam, B. Jongsomjit, and L. B. Juurlink, Molecules **19**, 10845 (2014).
[13] K. Besocke, B. Krahl-Urban, and H. Wagner, Surf. Sci. **68**, 39 (1977).
[14] H.-T. Liu, A. Armitage, and D. Woodruff, Surf. Sci. **114**, 431 (1982).
[15] A. Armitage, H. Liu, and D. Woodruff, Vacuum **31**, 519 (1981).
[16] M. Corso, F. Schiller, L. Fernandez, J. Cordón, and J. Ortega, J. Phys. Condens. Matter **21**, 353001 (2009).
[17] A. De Alwis, B. Holsclaw, V. Pushkarev, A. Reinicker, T. Lawton, M. Blecher, E. Sykes, and A. Gellman, Surf. Sci. **608**, 80 (2013).
[18] J. E. Ortega, M. Corso, Z. Abd-el Fattah, E. Goiri, and F. Schiller, Phys. Rev. B **83**, 085411 (2011).
[19] F. M. Hoffmann, Surf. Sci. Rep. **3**, 107 (1983).
[20] Y. J. Chabal, Surf. Sci. Rep. **8**, 211 (1988).
[21] R. G. Greenler, J. Chem. Phys. **50**, 1963 (1969).
[22] R. G. Greenler, J. Chem. Phys. **44**, 310 (1966).
[23] M. Van Hove and G. Somorjai, Surf. Sci. **92**, 489 (1980).
[24] Y. Suzaki and A. Tachibana, Appl. Opt. **14**, 2809 (1975).
[25] Thorlabs' Stabilized Tungsten IR Light Source with fiber adapter SLS202L, range 450 - 5500 nm.
[26] G. Ertl, *Reactions at solid surfaces*, Vol. 14 (John Wiley & Sons, 2010).
[27] J.-S. McEwen, S. Payne, H. J. Kreuzer, M. Kinne, R. Denecke, and H.-P. Steinrück, Surf. Sci. **545**, 47 (2003).
[28] H. Steininger, S. Lehwald, and H. Ibach, Surf. Sci. **123**, 264 (1982).
[29] A. Baro and H. Ibach, J. Chem. Phys. **71**, 4812 (1979).
[30] D. Ogletree, M. Van Hove, and G. Somorjai, Surf. Sci. **173**, 351 (1986).
[31] G. Ertl, M. Neumann, and K. Streit, Surf. Sci. **64**, 393 (1977).
[32] H. Yang, T. Minato, M. Kawai, and Y. Kim, J. Phys. Chem. C **117**, 16429 (2013).
[33] R. Ryberg, Phys. Rev. B **40**, 865 (1989).
[34] I. J. Malik and M. Trenary, Surf. Sci. Lett. **214**, L237 (1989).
[35] J. Xu and J. T. Yates, Surf. Sci. **327**, 193 (1995).
[36] R. Mukerji, A. Bolina, and W. Brown, Surf. Sci. **527**, 198 (2003).
[37] B. Tränkenschuh, N. Fritsche, T. Fuhrmann, C. Papp, J. Zhu, R. Denecke, and H.-P. Steinrück, J. Chem. Phys. **124**, 074712 (2006).
[38] B. Tränkenschuh, C. Papp, T. Fuhrmann, R. Denecke, and H.-P. Steinrück, Surf. Sci. **601**, 1108 (2007).
[39] S. Shimizu, H. Noritake, T. Koitaya, K. Mukai, S. Yoshimoto, and J. Yoshinobu, Surf. Sci. **608**, 220 (2013).
[40] J. Yoshinobu, N. Tsukahara, F. Yasui, K. Mukai, and Y. Yamashita, Phys. Rev. Lett. **90**, 248301 (2003).
[41] G. Blyholder, J. Phys. Chem. **68**, 2772 (1964).
[42] A. Crossley and D. A. King, Surf. Sci. **68**, 528 (1977).
[43] K. Horn and J. Pritchard, J. Phys. Colloq. **38**, 164 (1977).
[44] P. Hollins, Surf. Sci. Rep. **16**, 51 (1992).

[45]H. Froitzheim, H. Hopster, H. Ibach, and S. Lehwald, Appl. Phys. **13**, 147 (1977).